American Mineralogist, Volume 97, pages 281–290, 2012

Hanjiangite, a new barium-vanadium phyllosilicate carbonate mineral from the Shiti barium deposit in the Dabashan region, China

Jiajun Liu,[1,2,3,*] Guowu Li,[1] Qian Mao,[4] Shenghua Wu,[1,3] Zhenjiang Liu,[1,3] Shangguo Su,[1,3] Ming Xiong,[1] and Xiaoyan Yu[5]

[1]State Key Laboratory of Geological Processes and Mineral Resources, China University of Geosciences (Beijing), Beijing 100083, P.R. China
[2]State Key Laboratory of Ore Deposit Geochemistry, Institute of Geochemistry, Chinese Academy of Sciences, Guiyang 550002, P.R. China
[3]School of Earth Earth Science and Resources, China University of Geosciences (Beijing), Beijing 100083, P.R. China
[4]Institute of Geology and Geophysics, Chinese Academy of Sciences, Beijing 100029, P.R. China
[5]School of Gemology, China University of Geosciences (Beijing), Beijing 100083, P.R. China

Abstract

Hanjiangite, ideal formula $Ba_2Ca(V^{3+}Al)[Si_3AlO_{10}(OH)_2]F(CO_3)_2$, is a new mineral found in the Shiti barium deposit in the Dabashan region, China. Hanjiangite was collected from lenticular witherite ore bodies and witherite-barite-quartz veins cutting carbonaceous slates. It is found as disseminations in both settings. It occurs as thin, euhedral, tetragonal, tabular crystals, and anhedral grains. Grain size commonly varies from 0.05 to 4 mm and occasionally reaches 15 mm. It is yellow-green or dark green, with one well-developed or perfect cleavage on {001}. Other physical properties are: brittle, transparent to translucent, nonfluorescent, vitreous luster, greenish white streak, hardness 4 in the Mohs scale, splintery fracture, and a measured density of 3.69 g/cm^3. Hanjiangite is biaxial (–), $\alpha = 1.615$, $\beta = 1.655$, $\gamma = 1.700$ (589 nm), and displays strong pleochroism from pale yellow-green to dark green. It is monoclinic, with unit-cell parameters refined from single-crystal X-ray diffraction: $a = 5.2050(12)$, $b = 9.033(2)$, $c = 32.077(8)$ Å, $\beta = 93.49(8)°$, $V = 1505.4(8)$ Å^3, $Z = 4$, space group $C2$. The strongest seven lines of the X-ray powder-diffraction pattern [d in Å(I)(hkl)] are: 15.866(7)(002), 5.340(91)(006), 4.010(10)($\bar{1}$14), 3.209(23) (027), 2.676(100) ($\bar{1}$ 1 10), 2.294(29)($\bar{1}$37), and 2.008(11)($\bar{2}$28). Chemical analysis by a combination of electron microprobe, HF combustion, IR absorption, thermogravimetric analysis (TGA) and crystal-structure refinement gives SiO_2 19.64, TiO_2 1.12, Al_2O_3 11.19, MgO 0.54, CaO 4.91, BaO 34.89, V_2O_3 9.93, Cr_2O_3 1.75, Na_2O 0.20, K_2O 0.06, MnO 0.01, FeO 0.02, NiO 0.01, SrO 0.34, Y_2O_3 0.85, La_2O_3 0.14, Nd_2O_3 0.26, F 1.80, Cl 0.04, CO_2 10.37, H_2O 1.30, F=O –0.76, Cl=O –0.01, sum 98.60 wt%. The empirical formula is $(Ba_{1.98}Na_{0.06}K_{0.01})_{\Sigma 2.05}(Ca_{0.76}Mg_{0.12}Y_{0.06}Sr_{0.03}\ La_{0.01}Nd_{0.01})_{\Sigma 0.99}(V_{1.15}Al_{0.75}Cr_{0.20}Ti_{0.12})_{\Sigma 2.22}[(Si_{2.84}Al_{1.16})_{\Sigma 4.00}O_{10}][(OH)_{1.25}O_{0.77}]_{\Sigma 2.02}(F_{0.82}Cl_{0.01})_{\Sigma 0.83}(CO_3)_{2.05}$ based on 19 anions per formula unit. A single-crystal X-ray structure determination (sample 2005st-17) was carried out with a Smart APEX CCD system using Mo$K\alpha$ ($\lambda = 0.71073$ Å) radiation. The structure was solved using direct methods, and refined with the SHELXTL PC (Bruker AXS Inc.) package. Anisotropic refinement using all measured independent data and reflections with $I > 2\sigma(I)$ resulted in an R_1 factor of 0.08 and wR^2 of 0.20. The crystal structure is composed of alternating T-O-T and $Ba_2Ca(CO_3)_2F$ layers. The $Ba_2Ca(CO_3)_2F$ layer occurs between the T-O-T layers. The T site contains both Si and Al, and the O site both V^{3+} and Al. The interlayer hosts not only Ba (like in chernykhite) but also Ca atoms and (CO_3) groups. While the coordination of the cations in the TOT layer is obvious, the coordinations of Ca and Ba in the interlayer are not straight forward. A hanjiangite has three polytypes, namely 1*M*-type, 2*M*-type, and 3*T*-type.

Keywords: New mineral, hanjiangite, electron-microprobe data, single-crystal X-ray diffraction, crystal structure, Shiti barium deposit, Ankang County, China

Introduction

Hanjiangite was discovered in some ore samples from the Shiti barium deposit in southern Shaanxi, China. In the process of surveying the assemblage using backscattered electron (BSE) imaging and energy-dispersive X-ray spectrometry (EDS), a mineral with very unusual barium-rich chemistry was noticed. Subsequent quantitative electron microprobe analyses and single-crystal X-ray studies made it clear that this was a new mineral. The new mineral is named after the Hanjiang River, the largest branch of the Yangtze River, China. Many witherite and barite deposits are located at the vicinity of the middle to upper reaches of the Hanjiang River catchment and the Hanjiang River flows through the Shiti ore district. The new mineral and the name were approved by the International Mineralogical Association, Commission on New Minerals, Nomenclature and Classification (CNMNC) (IMA 2009-082).

Holotype material, including the polished thin section used for microprobe analyses, the single crystal used for the structure analysis, and a macro-crystal of hanjiangite have been deposited

* E-mail: liujiajun@cugb.edu.cn

0003-004X/12/0203–281$05.00/DOI: http://dx.doi.org/10.2138/am.2012.3781

at the Geological Museum of China, Beijing, China, specimen number M11740.

Geological setting

Barite ($BaSO_4$) deposits are widespread around the world, whereas witherite ($BaCO_3$) deposits are rarely reported. Numerous layered witherite and barite deposits are extensively developed in the Early Paleozoic silicate formations of southern Qinling Mountains in the Dabashan region at the boundary of Sichuan, Chongqing, Shaanxi, and Hubei provinces. These two types of deposits, representing a large-scale barium metallogenic belt, exhibit paragenetic and separated distribution characteristics (Liu et al. 2007, 2008a, 2010). The Shiti barite deposit is typical among these barium deposits.

The entire barium metallogenic belt is exposed on the northern side of the Dabashan arc fault, and it measures more than 300 km in length, extending from the Fushui River at Xixiang, Shaanxi in the north, southward into areas around Zhuxi and Zhushan of Hubei Province via Ziyang of Shaanxi, Wanyuan of Sichuan, Chengkou of Chongqing, and Zhenping of Shaanxi (Lv et al. 2003). At present, more than 70 witherite and barite or witherite-barite deposits have been discovered in this ore zone (Liu et al. 2010). These ore deposits, being stratiform or stratoid in form, are hosted in the Lower Cambrian and the Lower Silurian siliceous rocks, and are characterized by persisting synsedimentary ore beds. The orebodies are controlled by lithological character and petrography (Liu et al. 2007, 2008a, 2010; Wu et al. 2010a). In the past years, research has been done on ore-forming conditions and mechanisms of witherite-barite deposits hosted in the Lower Cambrian and Lower Silurian black rock series of the north Dabashan area. Various genetic models of formation for witherite and barite deposits, such as chemical synsedimentation (Tu 1999a), metasomatism (Lv et al. 2003), volcanogenic sedimentation (Tu 1999a, 1999b), biogenic (Gao 1998; Wang and Ye 1998; Fan et al. 2004) and hydrothermal sedimetation (Jiao 1994; Tang et al. 1998; Fang 1999), have been proposed. However, little information has been acquired about formation mechanisms of witherite and barite in the sedimentary environment. Based on evidence of the fluid inclusions and sulfur isotopes, the authors suggested that the solution thermochemical sulfate reduction (TSR) was the main metallogenic mechanism of formation of witherite deposits, and the formation of barite deposits are also closely associated with hydrothermal fluids (Liu et al. 2008a, 2008b, 2010).

Occurrence and associated minerals

Hanjiangite is found in the Shiti barium deposit in the Dabashan region, China (32°43'45" to 32°45'06"N 109°08'22" to 109°10'20"E). Shiti is a very large deposit located about 20 km east of Ankang County, Shaanxi Province, China (Wu et al. 2010b). The deposit is hosted by Lower Silurian carbonaceous cherts, slates, and sandstones (Liu et al. 2007, 2008a; Wu et al. 2010b). Hanjiangite was collected from lenticular witherite ore bodies and witherite-barite-quartz veins cutting carbonaceous slates. It is found as disseminations in both settings.

The deposit is mineralogically complex. Until now, more than 20 minerals have been identified in the ores, including sulfates, carbonates, sulfides, and oxides of Ba, Fe, V, As, Cu, Pb, Zn, etc. The most common minerals include witherite, barite, barytocalcite, chernykhite, sphalerite, pyrite, sulvanite, norsethite, quartz, and calcite, with minor celsian, siderite, ankangite, zoltaiite, vanoxite, karelianite, and duttonite. Closely associated hanjiangite are witherite, barite, barytocalcite, and quartz (Liu et al. 2008c). Hanjiangite occurs as a disseminated mineral with an estimated modal abundance of 0.01%.

A systematic study of fluid inclusions in associated witherite, barite, barytocalcite, and quartz shows that hanjiangite mainly formed between 120 and 220 °C based on homogenization temperatures. Gaseous phases are mainly CH_4, N_2, CO_2, and H_2S (Liu et al. 2008b, 2010; Wu et al. 2010b). This suggests that the mineral crystallized as a primary phase directly from hydrothermal fluids.

Physical and optical properties

Hanjiangite occurs as thin, euhedral, tetragonal, tabular crystals and anhedral grains. Grain size commonly varies from 0.05 to 4 mm and occasionally reaches 15 mm (Fig. 1).

Hanjiangite varies from yellow-green to dark green and has a well-developed or perfect cleavage on {001} (Fig. 1). The cleavable masses are brittle, transparent to translucent, nonfluorescent in short-wave ultraviolet light, and have a vitreous luster, splintery fracture, and a greenish white streak. Micro-hardness of five grains of hanjiangite ranges from 191 to 215 kg/mm^2, averaging 203 kg/mm^2 (for 25 g load), corresponding to a hardness of 4.00 in Mohs scale. A standard deviation calculated from five measurements is 203.21. The measured density is 3.69 g/cm^3 by pycnometry, similar to the calculated density of 3.78 g/cm^3 based on the empirical formula and cell dimensions derived from single-crystal X-ray diffraction study. A measurement error is ±0.11. A spindle stage was used to orient a crystal for measurement of indices of refraction and determination of $2V$ with extinction curves. In transmitted plane-polarized light, hanjiangite is strongly pleochroic with pale yellow-green to deep green, biaxial negative with $\alpha = 1.615$, $\beta = 1.655$, $\gamma = 1.700$ (measured at 589 nm using a GEM-A REF0006 refractometer by Xianyan Yu), $2V_{obs} = 114$~$115°$, $2V_{calc} = 88.8°$, medium dispersion $r > v$.

Application of the Gladstone-Dale relationship (Mandarino 1981) gives a compatibility index of 0.085 using the empirical formula and measured density, which is considered to be borderline fair to poor. The reason for this compatibility value is unknown at this time. It may be due to significant differences between indices of refraction of the crystal used for structure determination and that used for optical characterization, though it is possible that the constants given by Mandarino (1981) for some of the oxides may need to be revised for this particular type of silicate structure (Roberts et al. 2001).

Thermogravimetric analysis (TGA) and differential thermal analysis (DTA)

The thermogravimetry analysis (TGA) and the differential thermal analysis (DTA) were conducted in the temperature range from room temperature to 1000 °C using a Peking Simultaneous TGA/DTA instrument model Peking LCT-21 by Qinfang Fang at the State Key Laboratory of Geological Processes and Mineral Resources, China University of Geosciences. The sample mass of ~40 mg was contained in a platinum crucible and heated at a constant rate of 10 °C/min in flowing high-purity nitrogen. The TGA

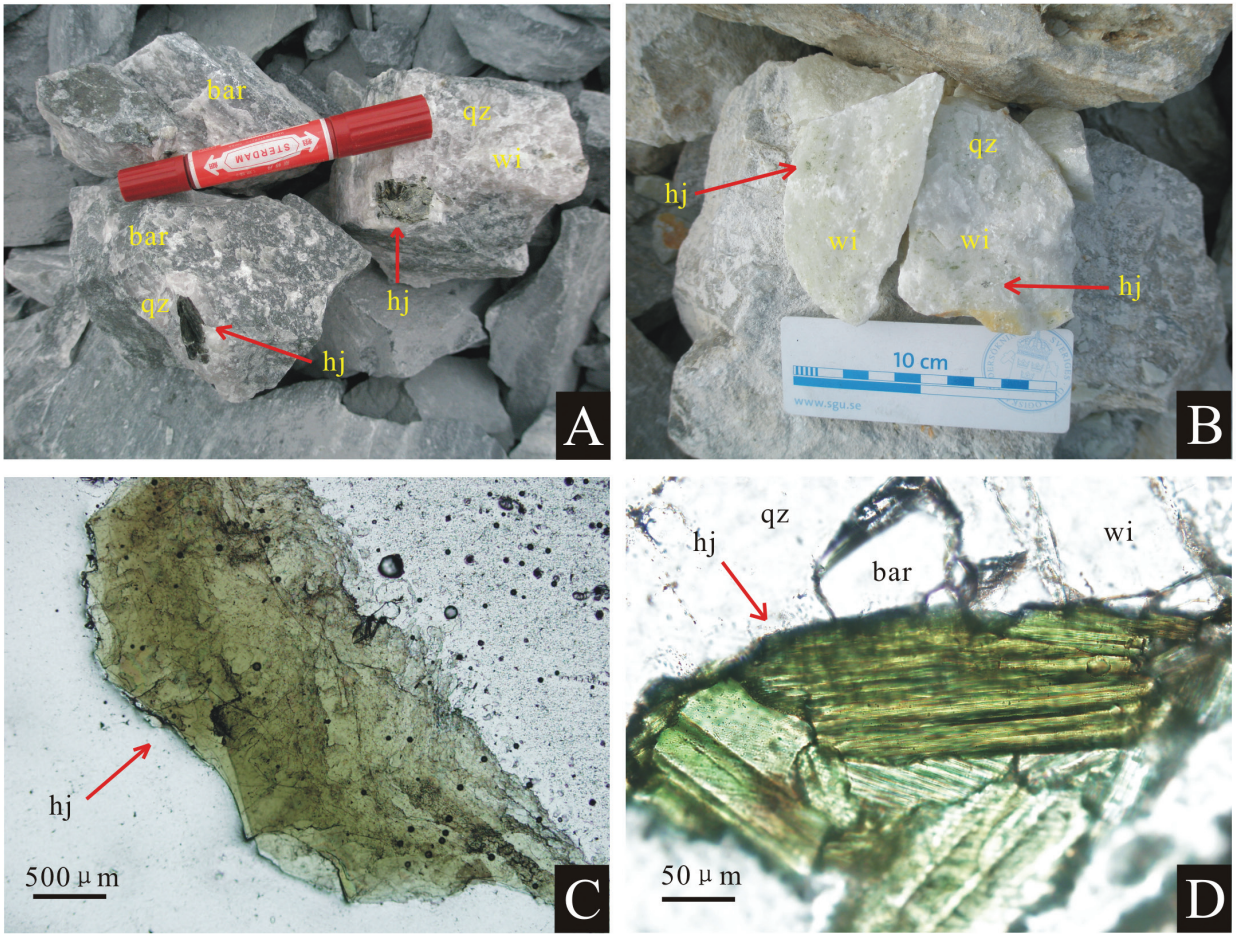

FIGURE 1. (**a** and **b**) Photographs of samples containing dark green flakes of hanjiangite (hj) occurring as inclusions in barite-witherite-quartz veins. (**c** and **d**) Photomicrographs of thin section under plane-polarized light (–) with hanjiangite showing its thin tabular habit; sample 2005st-17. Abbreviations: barite = bar; witherite= wi; quartz = qz.

and DTA curves for three hanjiangite samples in the temperature range from room temperature to 1000 °C are shown in Figures 2a, 2b, and 2c, respectively. TGA up to 1000 °C revealed that total weight losses at 790 °C are 11.61–11.65% for all samples of hanjiangite, in agreement with the theoretical hydroxyl (OH) and CO_2 contents of hanjiangite. The DTA curves of three samples of hanjiangite show two endothermic peaks at 656 °C (weak) and 770 °C (very strong) (shown in Fig. 2a), at 686 °C (weak) and 765 °C (very strong) (shown in Fig. 2b), and at 685 °C (weak) and 752 °C (very strong) (shown in Fig. 2c), respectively. There are two very small exothermic peak at 363–374 °C in the three DTA curves (shown in Figs. 2a, 2b, and 2c).

The TGA and DTA curves for the three hanjiangite samples share some general features (Fig. 2a, 2b, and 2c), such as: (1) very limited weight loss below 740 °C; (2) marked weight loss in the 740–790 °C range; and (3) the occurrence of a very strong endothermic and a weak endothermic DTA signals, systematically close to ~752–770 and ~656–686 °C, respectively. (4) The two weak exothermic peaks could not be assigned. The thermal data also indicate that H_2O molecules are not present in the structure of hanjiangite.

Infrared spectroscopy

Two samples of hanjiangite have been studied on a Perkin-Elmer FTIR spectrometer PE983G with a DTGS detector and a KBr beamsplitter by Yinxiang Zhao at the Key Laboratory of Orogen and Crust Evolution of Ministry of Education, Peking University. The material was crushed in a corundum mortar, mixed with KBr, and then pressed to pellets 13 mm in diameter. The spectra were recorded over a range from 4000 to 180 cm^{-1}. The infrared absorption spectrum of hanjiangite is shown in Figure 3. The transmittance spectra show very large, sharp peaks at 991 and 1437 cm^{-1}, medium sharp peak at 868 cm^{-1}, and a small sharp peak at 1780 cm^{-1} in Figure 3a, and very large sharp peaks at 986 and 1437 cm^{-1}, medium sharp peak at 869 cm^{-1}, and a small sharp peak at 1781 cm^{-1} in Figure 3b, confirming the presence of CO_3 groups in the structure (Basciano et al. 2001). In addition, the transmittance spectra show a weak peak at 1624 cm^{-1} shown in Figures 3a and 3b due to H-O-H bending, which might be indicative of the presence of a very small amount of H_2O molecules in the structure. In the case of hanjiangite, however, we may observe the existence of only one sharp peak at 3522 cm^{-1} in Figure 3a and at 3527 cm^{-1} in Figure 3b in the 3600 cm^{-1}

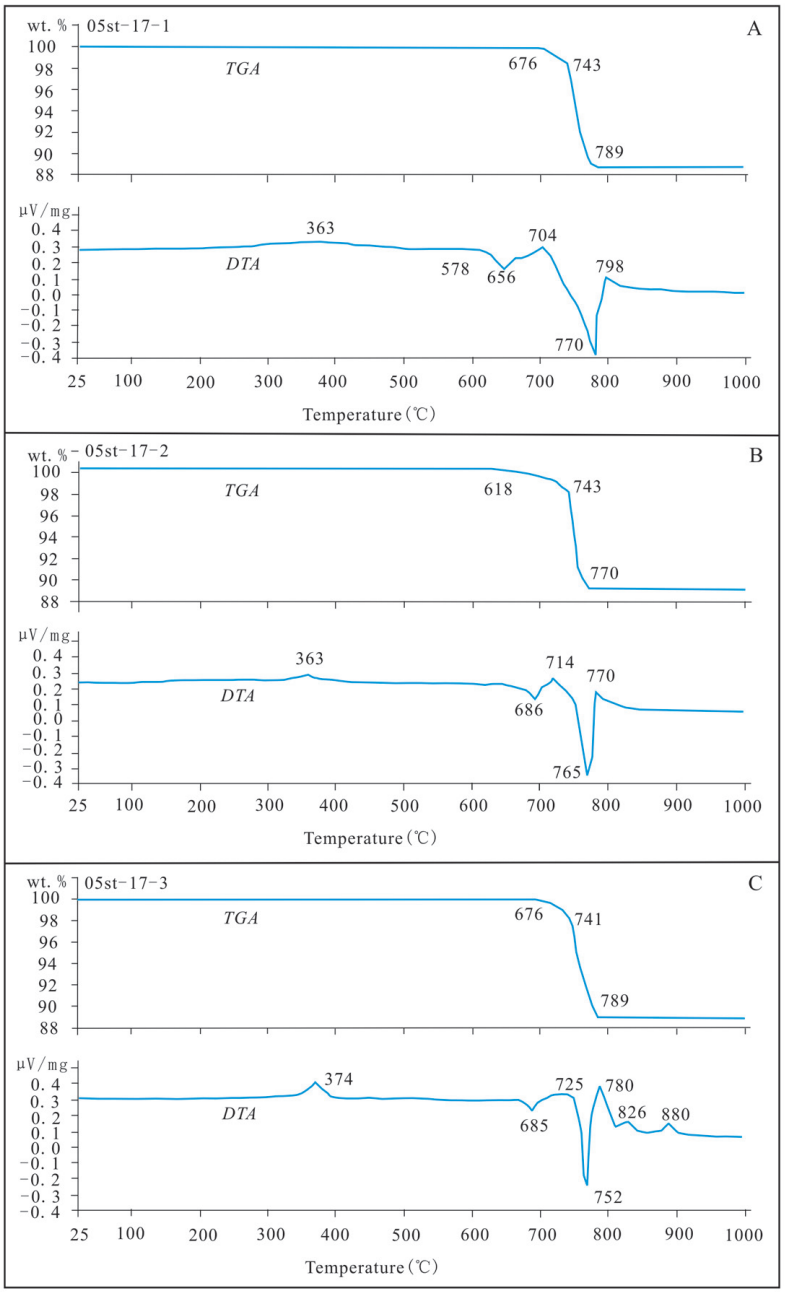

FIGURE 2. TGA and DTA curves of hanjiangite measured from room temperature to 1000 °C with a constant N_2 flow of 100 mL/min. The heating rate was 10 °C/min.

region of the spectra, which suggest that the water is mainly present as hydroxyl (OH) groups and not as H_2O molecules (Graeser et al. 2003). Such sharp peaks with small peak-widths are rarely seen in dioctahedral micas owing to the interactions of the hydroxyl groups with the two octahedrally coordinated Al atoms, and the high sensitivity of the stretching frequency of OH groups (Farmer 1974). Such sharp peaks have previously only been recorded in well-ordered structures of sheet silicates such as pyrophyllite or in regularly substituted celadonite, where the hydroxyl group is coordinated to a divalent and a trivalent cation (Farmer 1974). The sharpness of that peak in hanjiangite may be the result of a very high degree of hydroxyl-group order in the structure (Graeser et al. 2003).

Raman spectroscopy

The Raman spectrum of hanjiangite was recorded on a Renishaw RM1000 Raman system equipped with a CCD Peltier detector and a confocal argon laser (514.5 nm) by Jing Li at the Key Laboratory of Orogen and Crust Evolution of Ministry of Education, Peking University. The Raman system is connected to a Leica microscope to adjust the laser beam on the sample surface. The excitation spot was about 2 μm in size. An optical

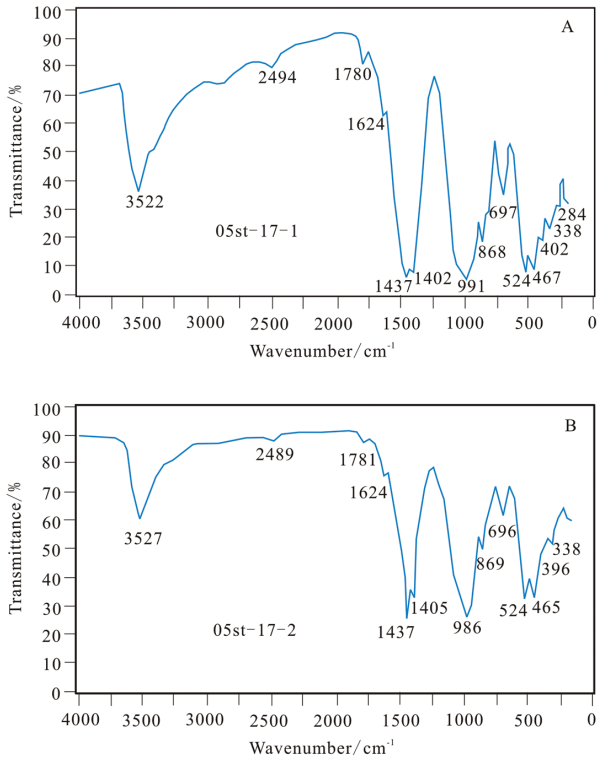

FIGURE 3. Infrared absorption spectra of hanjiangite.

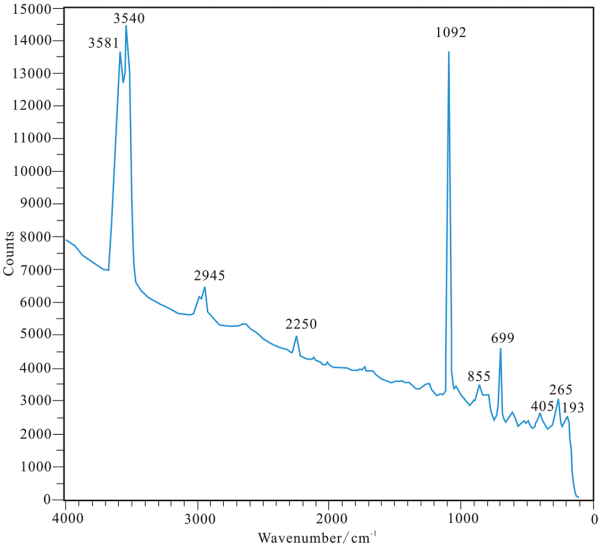

FIGURE 4. Raman spectra of hanjiangite.

magnification of 100× was used, and for each analysis, 50 scans were taken in the extended scan mode from 100 to 4000 cm^{-1} Raman shift. The data were recorded with GRAMS software. The accuracy of the detector is ±2 cm^{-1} for peaks. Raman spectra were collected in situ on single crystals of hanjiangite on polished thin section chips. The Raman spectrum of hanjiangite is shown in Figure 4. The Raman shift shows very strong sharp peaks at 1092, 3540, and 3581 cm^{-1}, medium sharp peak at 699, 2250, and 2945 cm^{-1} and weak sharp peaks at 193, 265, 405, and 855 cm^{-1} in Figure 4. A major peak at 1092 cm^{-1} and two minor peaks at 699 and 855 cm^{-1} show the presence of CO_3 groups in the structure (Vagenas and Kontoyannis 2003). The Raman shifts at 3540 and 3581 cm^{-1} are related to the O–H stretching mode, demonstrating the presence of hydroxyl (OH) groups in hanjiangite (Pasteris et al. 2004).

HF-COMBUSTION INFRARED ABSORPTION SPECTROSCOPY

The high-frequency combustion infrared absorption spectrometric analysis (HF-IR) was conducted in the temperature range from room temperature to 1500 °C using a LECO-CS 444 device by Li Yan at the National Analysis and Testing Center for Non-Ferrous Metals and Electronic Materials, China. The sample mass of ~50 mg was contained in a ceramic crucible and heated on a temperature ramp of 60 °C min^{-1} under flowing high-purity oxygen and nitrogen. The DOMTAR international gypsum standard (GYP-C) was used for calibration. The analytical methods are given in Yu and Ning (2002), Graeser et al. (2003), and Shi et al. (2001). Carbon and sulfur in range of ~0.1–3% can be determined accurately and their relative standard deviations are less than 2.6 and 3%, respectively (Song et al. 2002; Shi et al. 2001). Using the results of HF-combustion infrared absorption spectrometric analyses, the average concentration of carbon and sulfur in hanjiangite were calculated to be 2.83 and 0.00%, respectively, which gives a CO_2 content of 10.37 wt%.

CHEMICAL COMPOSITION

The microchemical composition of hanjiangite was determined using a JEOL JXA-8100 WDS-microprobe, at the Institute of Geology and Geophysics, Chinese Academy of Sciences. Operating conditions were 15 kV accelerating voltage, 10 nA beam current, and 30 μm beam diameter. The counting times were between 10 and 20 s on both peak and background. Standards, spectral lines, and crystals used were: kaersutite (Si*K*α, TAP; Fe*K*α, LIF), benitoite (Ti*K*α, LIF; Ba*L*α, PET), jadeite (Al*K*α, TAP; Na*K*α, TAP), K-feldspar (K*K*α, PET), bustamite (Mn*K*α, LIF), bustamite (Ca*K*α, PET), MgO (Mg*K*α, TAP), V_2O_5 (V*K*α, LIF), NiO (Ni*K*α, LIF), Cr_2O_3 (Cr*K*α, LIF), tugtupite (Cl*K*α, PET), CaF (F*K*α, LDE1), celestite (Sr*K*α, PET), Yalgrt (Y*K*α, TAP), LaP_5O_{14} (La*K*α, LIF), and NdP_5O_{14} (Nd*K*α, LIF). As mentioned above, total carbon was determined by the HF combustion IR absorption method and is 2.83 wt%. The H_2O content has been determined from the thermogravimetric analysis (TGA) data and is 1.3 wt%, which was checked by the structural model, assuming that water is present in hanjiangite only as OH groups. FTIR spectroscopy and Raman spectroscopy showed only OH, and no H_2O, in the studied sample. These spectroscopic studies also show the presence of some CO_3 groups (see above).

The average composition of hanjiangite, with the standard deviation and range, and the relevant standards used for calibration of the electron microprobe, are given in Table 1. The electron-microprobe data reported in Table 1 were calculated on the basis of 44 analyses carried on three different samples (seeing Appendix Table[1]). A ZAF-type correction procedure was used for all data reductions, and all iron was assumed to be ferrous. The chemical formula of hanjiangite was calculated on the basis of 19 atoms of anion per formula unit (Table 1). Results of some

TABLE 1. Results of electron-microprobe analyses of hanjiangite

	wt%	Range	Std. dev.		apfu	Probe standard
SiO_2	19.64	18.97–20.21	0.24	Si	2.840	kaersutite
TiO_2	1.12	0.96–1.24	0.06	Ti	0.122	benitoite
Al_2O_3	11.19	10.81–11.63	0.16	Al	1.907	jadeite
MgO	0.54	0.46–0.69	0.06	Mg	0.116	MgO
CaO	4.91	4.71–5.21	0.11	Ca	0.761	bustamite
BaO	34.89	34.26–35.84	0.42	Ba	1.977	benitoite
V_2O_3	9.93	9.51–10.19	0.16	V	1.151	V_2O_5
Cr_2O_3	1.75	1.54–1.88	0.08	Cr	0.200	Cr_2O_3
Na_2O	0.20	0.08–0.52	0.10	Na	0.056	jadeite
K_2O	0.06	0.00–0.14	0.02	K	0.011	K–feldspar
MnO	0.01	0.00–0.07	0.02	Mn	0.001	bustamite
FeO	0.02	0.00–0.12	0.02	Fe	0.002	kaersutite
NiO	0.01	0.00–0.09	0.02	Ni	0.002	NiO
SrO	0.34	0.00–0.73	0.21	Sr	0.029	celestite
$Y2O_3$	0.85	0.75–0.96	0.05	Y	0.065	$Y_3Al_5O_{12}$
La_2O_3	0.14	0.00–0.51	0.18	La	0.007	LaP_5O_{14}
Nd_2O_3	0.26	0.00–0.64	0.28	Nd	0.013	NdP_5O_{14}
F	1.80	1.70–1.89	0.05	F^-	0.823	CaF
Cl	0.04	0.00–0.14	0.05	Cl^-	0.010	tugtupite
CO_2*	10.37			CO_3^{2-}*	2.047	
H_2O†	1.30			OH^-†	1.254	
F = O	–0.76					
Cl = O	–0.01					
Total	98.60					

* Total carbon was determined by the HF combustion IR absorption method.
† The H_2O content has been determined from the thermogravimetric analysis (TGA) data and checked by the structural model.

TABLE 2. Indexed powder XRD data for hanjiangite

h	*k*	*l*	I/I_0(%)	d_{obs} (Å)	d_{calc} (Å)	2Th(°)*
0	0	2	7	15.866	16.014	0.051
0	0	4	1	7.993	8.007	0.020
0	0	6	91	5.340	5.338	–0.007
0	2	1	<1	4.459	4.469	0.044
1	1	4	10	4.010	4.017	0.039
0	2	5	1	3.706	3.690	–0.112
0	0	9	1	3.552	3.559	0.048
1	1	6	1	3.356	3.356	–0.001
0	2	7	23	3.209	3.213	0.036
1	1	7	<1	3.123	3.128	0.046
1	1	10	100	2.676	2.678	0.023
2	0	1	1	2.600	2.602	0.027
1	3	2	<1	2.554	2.558	0.056
2	0	4	<1	2.518	2.517	–0.015
1	3	4	1	2.456	2.454	–0.023
2	0	5	<1	2.362	2.358	–0.061
1	3	7	29	2.294	2.293	–0.016
0	4	4	<1	2.172	2.172	0.010
2	2	5	<1	2.092	2.090	–0.039
2	2	8	11	2.008	2.008	0.014
0	4	11	1	1.785	1.784	–0.046
1	3	14	<1	1.747	1.745	–0.059
2	4	3	<1	1.694	1.693	–0.044
2	0	16	<1	1.634	1.635	0.016
0	4	14	4	1.607	1.607	–0.011
1	5	7	<1	1.586	1.588	0.069
3	3	4	2	1.461	1.462	0.031

* $2Th(°) = 2\theta_{obs} - 2\theta_{calc}$.

of the individual analyses are shown in Appendix Table[1]; their H_2O content has not been analytically determined. An idealized anion group is assumed, and the stoichometry was calculated on the basis of 19 anions per formula unit according to the results of the single-crystal X-ray structure. The empirical formula is $(Ba_{1.98}Na_{0.06}K_{0.01})_{\Sigma 2.05}(Ca_{0.76}Mg_{0.12}Y_{0.06}Sr_{0.03}La_{0.01}Nd_{0.01})_{\Sigma 0.99}(V_{1.15}Al_{0.75}Cr_{0.20}Ti_{0.12})_{\Sigma 2.22}[(Si_{2.84}Al_{1.16})_{\Sigma 4.00}O_{10}][(OH)_{1.25}O_{0.77}]_{\Sigma 2.02}(F_{0.82}Cl_{0.01})_{\Sigma 0.83}(CO_3)_{2.05}$. This gives the total positive charge of 37.162 and the total negative charge of 37.167. The simplified formula is $Ba_2Ca(V^{3+}Al)[Si_3AlO_{10}(OH)_2]F(CO_3)_2$, and the ideal formula is $Ba_2CaV_2^{3+}[(Si_3AlO_{10})(OH)_2]F(CO_3)_2$.

Backscattered electron (Fig. 5a) and X-ray scanning spectroscopy maps for Ba, V, Si, Al, and Ca (Figs. 5b, 5c, 5d, 5e, and 5f, respectively) show that the above mentioned elements are uniformly distributed throughout hanjiangite. (CIF available on deposit[1].)

X-ray diffraction

Powder X-ray data. The X-ray powder diffraction pattern of hanjiangite was collected using a Rigaku D/Max-2500 X-ray diffractometer at the Research Institute of Petroleum Exploration and Development, China (Table 2), with graphite monochromatized Cu*K*α X-radiation (λ = 1.54178 Å). Peak intensities were measured with an automated densitometer and the pattern was indexed on the basis of the powder spectra calculated on the basis of the result of the structural study (see below). The indexed powder diffraction data and estimated standard deviation to the observed *d*-values for hanjiangite are listed in Table 2. The seven strongest lines of the X-ray powder-diffraction pattern [*d* in Å(*I*)(*hkl*)] are: 15.866(7)(002), 5.340(91)(006), 4.010(10)($\bar{1}$14), 3.209(23)(027), 2.676(100)($\bar{1}$ 1 10), 2.294(29)($\bar{1}$37), and 2.008(11)($\bar{2}$28).

Single-crystal X-ray data. A crystal (sample 2005st-17) of 25 × 15 × 2 μm was used for single-crystal X-ray diffraction using a Bruker AXS SMART APEX diffractometer equipped with a CCD detector, working at 45 kV and 35 mA, at the State Key Laboratory of Geological Processes and Mineral Resources, China University of Geosciences (Beijing). A hemisphere of data was collected using graphite-monochromatized Mo*K*α (λ = 0.71073 Å) radiation and frame widths of 0.3° in ω, with 10 s per frame exposure time. Data were collected at room temperature. The structure was solved by direct methods, and the refinement was conducted with the SHELXTL PC (Bruker AXS Inc.) package. A subset of reflections accounting for nearly half of the total number of reflections was identified that obeyed a single orientation matrix and gave a monoclinic unit cell with *a* = 5.2050(12), *b* = 9.033(2), *c* = 32.077(8) Å, β = 93.49(8)°, *V* = 1505.4(8) Å^3, *Z* = 4, Space group *C*2. The *a*:*b*:*c* ratio calculated from the unit-cell parameters is 0.576:1:3.551. A summary of the data collection is presented in Table 3.

Structure refinement

Anisotropic refinement using all measured independent data and reflections with $I > 2\sigma(I)$ resulted in an R_1 factor of 0.08 and wR^2 of 0.20. Atom coordinates and site occupancy factors and selected bond lengths are given in Tables 4 and 5.

DISCUSSION

The crystal structure

The properties of hanjiangite strongly suggest that the mineral can be regarded as composed of a 2:1 layer of TOT (tetrahedral-octahedral-tetrahedral) incorporating a $Ba_2CaF(CO_3)_2$ interlayer. The interlayer space is wide. In fact, it is built up by alternat-

[1] Deposit item AM-12-011, Appendix table and CIF. Deposit items are available two ways: For a paper copy contact the Business Office of the Mineralogical Society of America (see inside front cover of recent issue) for price information. For an electronic copy visit the MSA web site at http://www.minsocam.org, go to the *American Mineralogist* Contents, find the table of contents for the specific volume/issue wanted, and then click on the deposit link there.

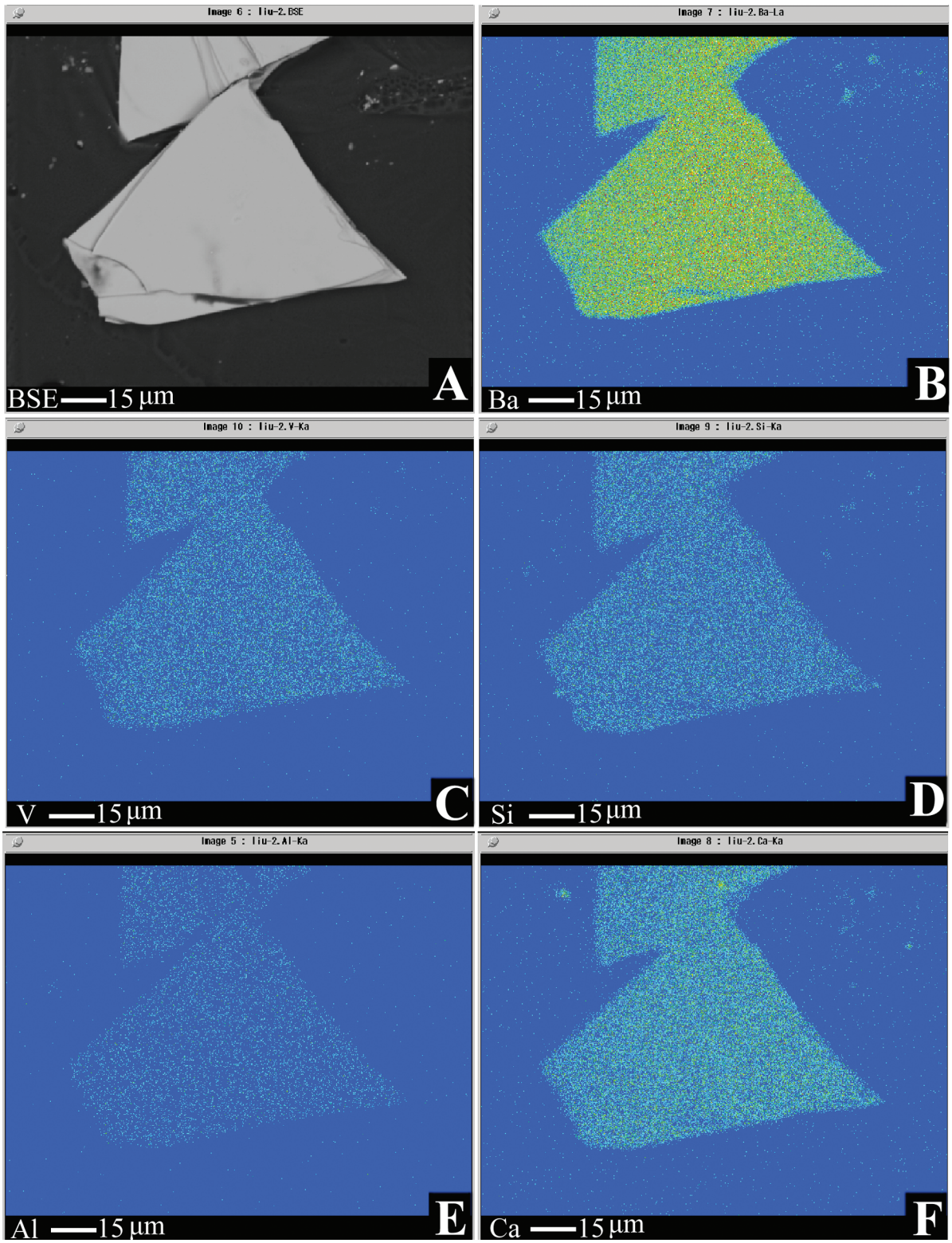

FIGURE 5. (**a**) Backscattered-electron (BSE) micrograph. (**b**, **c**, **d**, **e**, and **f**) X-ray scanning images of Ba, V, Si, Al, and Ca elements of a hanjiangite grain, respectively.

ing "pyrophyllite-like" layers $[AlV^{3+}Si_3AlO_{10}(OH)_2]^{1-}$ and $[Ba_2CaF(CO_3)_2]^{1+}$ layers. The tetrahedral site (T site) contains both Si and Al, and the octahedral site (O site) both V^{3+} and Al^{3+}. The arrangement is different to that found in pyrophyllite, namely the T layer is a ditrigonal-pyramid instead of a hexagon in hanjiangite (see Figs. 6–9).

The refinements of the hanjiangite structure suggest that there are two kinds of Al coordination, namely sixfold- and fourfold-coordinated atoms. The octahedral Al is disordered within the $V^{3+}O_6$ octahedral sheet, while the tetrahedral Al, substitutes in an ordered way for half of the Si^{4+} on the Si2 and Si3 sites (see Table 4). The Si to Al ratio is therefore 3:1, forming $AlSi_3O_{10}$ silicate sheets, charge balanced by interlayer cations.

The barium-calcium carbonate fluoride layer interlayer has the composition $Ba_2CaF(CO_3)_2$. The interlayer structure is similar to the single-layer witherite structure. The cationic arrangement is similar to calcite, whereas the anionic arrangement is similar to aragonite. The difference is observed in the interlayer, where instead of only Ba (like in chernykhite) there are also Ca atoms and (CO_3) groups. While the coordination of the cations in the TOT layer is regular, the coordinations of Ca and Ba in the interlayer are not straight forward. Barium atoms center 10-fold polyhedra, which are linked to the terminal oxygen in the tetrahedral sheet, an oxygen in the (CO_3) groups and the F^- anions, respectively. Calcium atoms center eightfold polyhedra, which are only linked to the oxygen in the (CO_3) groups. The F^- anions are located in channels formed by Ca and (CO_3) groups of the interlayer framework. The presence of F^- anions in this last layer is supported by the occurrence of F^- in barium calcium carbonates such as podlesnoite $[BaCa_2(CO_3)_2F_2]$ (Pekov et al. 2008).

The presence of the hydroxyl groups in the structure of Hanjiangite is clearly confirmed by the infrared and Raman spectra. The hydroxyl groups may be placed in the dioctahedral layer at the O5 and O7 sites, which are not linked to the Si cations. The other possible position for OH^- and F^- anions would be at sites F1 and F2, which are linked to Ba1 and Ba2 cations, respectively. The F1 and F2 sites are coordinated by five cations in a trigonal bipyramidal coordination, namely 3 Ca cations in

TABLE 3. Crystal data and refinement parameters for hanjiangite

Crystal size (μm)	25 × 15 × 2
Crystal color	yellow-green
Space group	*C*2
a (Å)	5.2050(12)
b (Å)	9.033(2)
c (Å)	32.077(8)
V (Å³)	1505.4(8)
β	93.49(8)°
Z	4
Density (g/cm³)	3.69* (meas) ±0.11, 3.78(calc)
Diffractometer	Bruker AXS SMART APEX CCD
Scan mode Δω = Δφ(°)	0.3
T (K)	293
$2\theta_{max}$ (°)	26.37
hkl (total)	3530
hkl (unique) ($\|F_o\| > 4\sigma F_o$)	2640 [R_{int} = 0.0499]
R	0.07
wR^2	0.20

* Density measured by pycnometry.

TABLE 4. Final atomic coordinates, equivalent isotropic displacement parameters, and site occupancy factors for hanjiangite

Atom	Wyck.	Occ.	x/*a*	y/*b*	z/*c*	U_{eq}
Ba1	4*c*		0.9633(2)	0.53412(14)	0.41574(4)	0.012(1)
Ba2	4*c*		0.5259(3)	0.2288(2)	0.08458(6)	0.036(1)
Ca1	2*b*		1/2	0.3639(7)	1/2	0.016(1)
Ca2	2*a*		–1/2	0.5643(7)	0	0.017(2)
V1	4*c*	0.631	0.7416(8)	0.0509(6)	0.25013(13)	0.012(1)
Al1	4*c*	0.37	0.7416(8)	0.0509(6)	0.25013(13)	0.012(1)
V2	4*c*	0.693	1.2401(7)	0.2147(6)	0.25025(14)	0.015(1)
Al2	4*c*	0.31	1.2401(7)	0.2147(6)	0.25025(14)	0.015(1)
Si1	4*c*		1.4348(14)	–0.2932(9)	0.3357(2)	0.014(1)
Si2	4*c*	0.5	0.9262(14)	–0.1185(9)	0.3360(3)	0.016(1)
Al3	4*c*	0.5	0.9262(14)	–0.1185(9)	0.3360(3)	0.016(1)
Si3	4*c*	0.5	1.0353(12)	0.0586(7)	0.1648(3)	0.015(1)
Al4	4*c*	0.5	1.0353(12)	0.0586(7)	0.1648(3)	0.015(1)
Si4	4*c*	0.98	1.5510(13)	–0.1093(9)	0.1647(2)	0.013(2)
O1	4*c*		1.221(3)	–0.173(3)	0.3514(7)	0.013(4)
O2	4*c*		0.722(3)	–0.239(2)	0.3562(6)	0.010(3)
O3	4*c*		0.886(3)	0.043(3)	0.3569(5)	0.019(3)
O4	4*c*		0.880(3)	–0.115(2)	0.2847(5)	0.016(1)
O5	4*c*		0.431(3)	0.0681(18)	0.2829(5)	0.016(1)
O6	4*c*		0.938(3)	0.198(2)	0.2844(6)	0.016(1)
O7	4*c*		0.543(3)	0.208(2)	0.2176(6)	0.016(1)
O8	4*c*		1.038(3)	0.0702(19)	0.2163(5)	0.016(1)
O9	4*c*		0.599(3)	–0.117(2)	0.2154(6)	0.016(1)
O10	4*c*		1.088(3)	0.223(2)	0.1444(6)	0.025(3)
O11	4*c*		0.760(3)	–0.004(2)	0.1436(7)	0.025(3)
O12	4*c*		1.259(3)	–0.055(2)	0.1495(7)	0.027(4)
O13	4*c*		0.015(4)	0.257(2)	0.0482(8)	0.023(5)
O14	4*c*		–0.194(3)	0.468(3)	0.0519(7)	0.034(4)
O15	4*c*		0.237(3)	0.459(2)	0.0484(7)	0.035(4)
O16	4*c*		0.482(3)	0.5575(18)	0.4502(5)	0.022(3)
O17	4*c*		0.270(3)	0.772(2)	0.4492(6)	0.022(4)
O18	4*c*		0.689(3)	0.770(2)	0.4497(6)	0.022(3)
F1	2*a*	0.6	1/2	0.196(5)	0	0.037(6)
F2	2*b*	0.72	0	0.522(7)	1/2	0.05(11)
C1	4*c*		0.475(5)	0.703(3)	0.4516(8)	0.024(3)
C2	4*c*		0.014(5)	0.395(3)	0.0500(8)	0.024(3)

TABLE 5. Selected bond lengths (Å) for hanjiangite

Ba1-F2^{i}	2.700(3)	V1-O7^{ii}	1.01(2)
Ba1-O18	2.820(20)	V1-O8	1.950(20)
Ba1-O17^{i}	2.850(20)	V1-O5^{ii}	1.990(20)
Ba1-O16	2.807(17)	V1-O6	1.970(18)
Ba1-O17^{ii}	2.811(16)	V1-O9^{v}	1.998(19)
Ba1-O18^{i}	2.847(18)	V1-O4^{v}	1.974(18)
Ba1-O16^{ii}	2.862(16)		
Ba1-O3^{i}	2.986(18)	V2-O8	1.964 (17)
Ba1-O1^{iii}	3.006(24)	V2-O7	1.946(18)
Ba1-O2	3.022(18)	V2-O9	2.000(19)
		V2-O5	1.926(17)
Ba2-F1	2.724(5)	V2-O4	2.005(18)
Ba2-O14	2.795(25)	V2-O6	1.964(17)
Ba2-O15^{iv}	2.799(25)		
Ba2-O13^{iv}	2.850(22)	Si1-O1	1.655(24)
Ba2-O14^{v}	2.842(24)	Si1-O6^{i}	1.649(20)
Ba2-O13^{v}	2.876(23)	Si1-O3^{i}	1.654(27)
Ba2-O15	2.941(19)	Si1-O2^{ii}	1.669(18)
Ba2-O11^{vi}	3.035(20)		
Ba2-O12^{iii}	3.052(20)	Si2-O3	1.604(19)
Ba2-O10^{vii}	3.068(19)	Si2-O4	1.649(19)
Ca1-O16^{viii}	2.367(17)	Si2-O1	1.679(20)
Ca1-O16	2.367(17)		
Ca1-O18^{iii}	2.372(18)	Si3-O10	1.652(20)
Ca1-O18^{ix}	2.372(18)	Si3-O11	1.648(18)
Ca1-O17^{i}	2.366(19)	Si3-O8	1.654(19)
Ca1-O17^{x}	2.366(19)	Si3-O12	1.649(19)
Ca2-O15^{xii}	2.334(21)	Si4-O11^{i}	1.624(20)
Ca2-O15^{xi}	2.334(21)	Si4-O9^{i}	1.632(20)
Ca2-O14^{xiii}	2.396(21)	Si4-O12	1.643(18)
Ca2-O14	2.396(21)	Si4-O10^{ii}	1.665(20)
Ca2-O13^{iv}	2.326(22)		
Ca2-O13^{xiv}	2.326(22)	C2-O13	1.248(33)
		C2-O14	1.272(33)
		C2-O15	1.301(31)
		C1-O16	1.316(32)
		C1-O17	1.234(31)
		C1-O18	1.272(31)

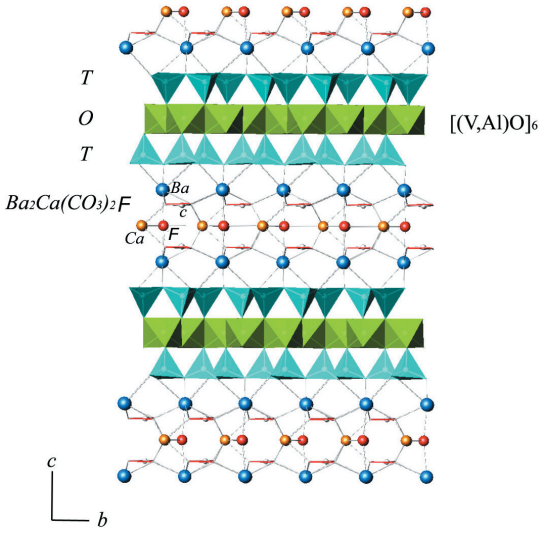

FIGURE 6. The crystal structure of hanjiangite as seen down **a**, with indication of the alternating TOT, namely $(VAl)Si_3AlO_{10}(OH)_2$ and $Ba_2Ca(CO_3)_2F$ layers.

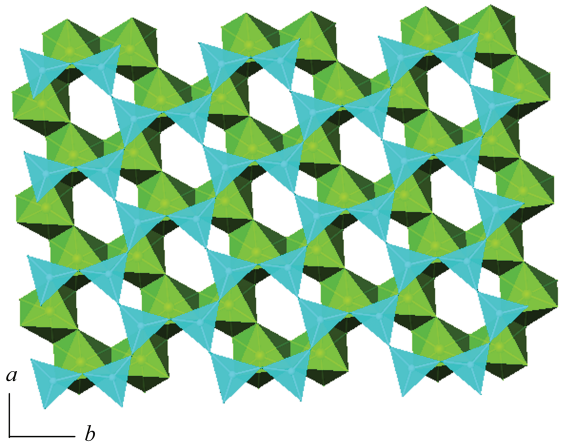

FIGURE 7. The TOT layer viewed in the direction normal to (001).

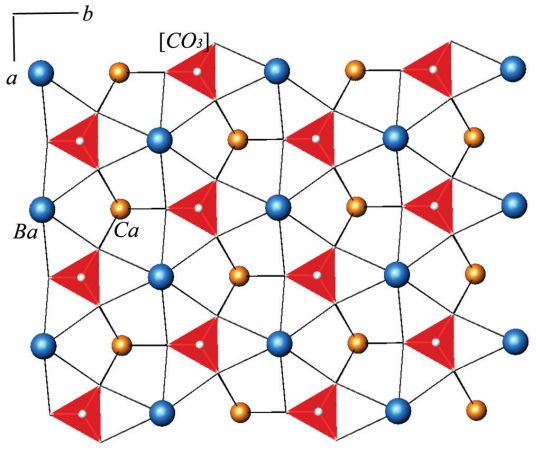

FIGURE 8. The $Ba_2Ca(CO_3)_2F$ layer viewed in the direction normal to (001).

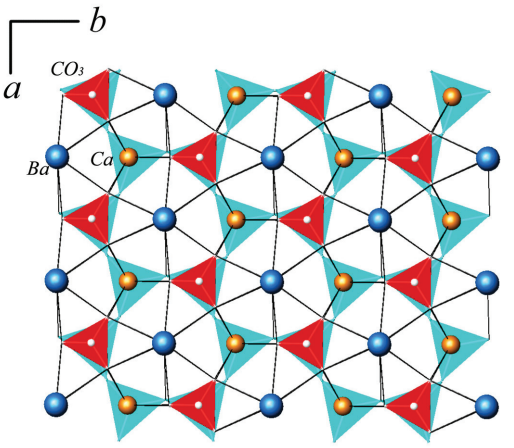

FIGURE 9. The $Ba_2Ca(CO_3)_2F$ layer superimposed on the T layer, viewed in the direction normal to (001).

TABLE 6. Comparison of some structural and physical properties between hanjiangite, surite, and chernykhite

	Hanjiangite*	Surite†	Chernykhite‡
Space group	*C*2	$P2_1$	*C*2/*c*
	Unit-cell parameters		
a	5.2050(12)	5.22	5.29
b	9.033(2)	8.97	9.182
c (Å)	32.077(8)	16.34	20.023
β	93.49(8)°	96.1°	95.68°
V (Å^3)	1505.4(8)		967.80
Z	4	2	4
d_{meas}	3.69	4.0 g/cm^3	~3.14–3.16
d_{calc}	3.780 g/cm^3		3.1 g/cm^3
	Strongest lines in the powder pattern (Å)		
	2.676(100)	4.05 (100)	3.33(100)
	5.340(91)	5.4 (71)	2.607(70)
	2.294 (29)	16.2 (68)	1.996(60)
	3.209(23)	3.24 (60)	1.660(60)
	4.010(10)	2.313 (50)	3.01(50)
	2.008(11)	2.700 (35)	1.530(50)
		4.48 (20)	2.887(40)
	Optical data		
	Biaxial (–)	Biaxial (–)	Biaxial (–)
α	1.615	1.693(2)	~1.640–1.643
β	1.655	n.d.	~1.686–1.691
γ	1.700	1.738(2)	~1.702–1.704
$2V_{meas}$	114–115~25°	n.d.	~11–12°

* Ideal chemical formula: $Ba_2CaV^{3+}(Si_3AlO_{10})(OH)_2F(CO_3)_2$.
† $Pb_{1.8}(Ca,Na)(Al,Fe,Mg)_2[Si_3AlO_{10}(OH)_2](CO_3)_2(H_2O)$.
‡ $(Ba,Na)(V^{3+},Al)_2(Si,Al)_4O_{10}(OH)_2$.

the central plane, with long bond distances, and 2 Ba cations as apical ligands at nearly 2.70 Å; therefore the two F1 and F2 sites correspond to F^- anions.

The crystal structure of hanjiangite may render itself to distinct polytypic variants (Merlino, personal communication):

Polytype 2*M* (the phase studied in this paper), $a = 5.205$, $b = 9.033$, $c = 32.077$ Å; $\beta = 93.49°$, space group *C*2.

Polytype 1*M*, $a = 5.205$, $b = 9.033$, $c = 16.10$ Å, b = 96.2°, space group *C*2.

Polytype 3*T*, $a = b = 5.205$, $c = 48.03$ Å, space group $P3_1$.

Relation to other species

Hanjiangite can be compared with chernykhite discovered by Ankinovich (Ankinovich 1973; Rozhdestvenskaya and Frank-Kamenetskii 1974; Rozhdestvenskaya 1979) with respect to physical and optical properties such as dark-green flake, well-developed or perfect cleavage, brittle, splintery fracture and a greenish white streak, transparent to translucent, vitreous luster, nonfluorescent, biaxial (–), but has a different chemical composition and crystal structure (Table 6).

Another mineral that presents the same typical features of hanjiangite, namely the alternation of a TOT layers and a carbonate layers is the mineral surite. Its structure is still unknown, but we may guess a close relationship between the two phases on the basis of crystallographic and chemical data. In fact, the unit cell of surite, monoclinic with $a = 5.22$, $b = 8.97$, $c = 16.3$ Å, $\beta = 96.1°$ (Table 6), is very similar to that of a possible polytype 1*M* of hanjiangite as described above.

Acknowledgments

Funding for this project was jointly granted the Major Basic Research Program of People's Republic of China (grant no. 2009CB421003 and 2009CB421005), by the National Natural Science Foundation of China (grant no. 41173062 and 40573032), by Program for Changjiang Scholars and Innovative Research Team in University (grant no. IRT0755), and by the 111 Project under the Ministry of Education and the State Administration of Foreign Experts Affairs, China (grant no. B07011). The authors thank Jingwu Yin, Jinhua Hao, Huarong Chen, and Xiang Gao of the China University of Geosciences (Beijing) for initial electron microprobe and initial X-ray diffraction analyses, and Yinxiang Zhao of Peking University for the infrared absorption spectroscopy study. We are indebted to Shengrong Li, Pu Wang, and Daisheng Sun of the China University of Geosciences (Beijing), and Jianchang You of the Research Institute of Petroleum Exploration and Development for their help. This manuscript has benefited from the comments and modifications of Peter A. Williams at the School of Natural Sciences, University of Western Sydney, Australia, and Steve D. Scott at the University of Toronto, Canada. This manuscript has also benefited from the comments, critical reviews and modifications from three referees, Stefano Merlino, and AE Andrew McDonald.

References cited

Ankinovich, S.G. (1973) Chernykhite, a new barium–vanadium mica from northwestern Karatau. International Geology Reviews, 15, 641–647.

Basciano, L.C., Groat, L.A., Roberts, A.C., Grice, J.D., Dunning, G.E., Foord, E.E., Kjarsgaard, I.M., and Walstrom, R.E. (2001) Kampfite, a new barium silicate carbonate mineral species from Fresno County, California. The Canadian Mineralogist, 39, 1053–1058.

Fan, D.L., Zhang, T., and Ye, J. (2004) Black shale series and its related ore deposit in China. Science Press, 131–184 (in Chinese).

Fang, W.X. (1999) Discussion on model of fluid dynamics for hydrothermal water system and geochemical patterns of paled hydrothermal fluids in the Qinling Orogen—The analysis and approach of sedimentary basin with hydrothermal sedimentation (Part II). Northwest Geoscience, 20, 17–27 (in Chinese with English abstract).

Farmer, V.C. (1974) The layer silicates. In V.C. Farmer, Ed., The Infrared Spectra of Minerals, p. 331–363. Mineralogical Society, London.

Gao, H.Z. (1998) The biochemical sedimentary metallogenic model of baritic and witheritic deposits in Lower Cambrian in China. Journal of Mineralogy and Petrology, 18, 70–77 (in Chinese with English abstract).

Graeser, S., Hetherington, C.J., and Giere, R. (2003) Ganterite, a new barium-dominant analogue of muscovite from the Berisal complex, Simplon region, Switzerland. The Canadian Mineralogist, 41, 1271–1280.

Hayase, K., Dristas, J.A., Tsutsumi, S., Otsuka, R., Tanabe, S., Sudo, T., and Nishiyama, T. (1978) Surite, a new Pb-rich layer silicate mineral. American Mineralogist, 63, 1175–1181.

Jiao, S.P. (1994) Formation conditions and genesis of the Bashan superlarge barium deposit, Chengkou County, Sichuan, China. Geotectonica et Metallogenia, 18, 110–111 (in Chinese with English abstract).

Kampf, A.R., Jackson, L.L., Sidder, G.B., Foord, E.E., and Adams, P.M. (1992) Ferrisurite, the Fe^{3+} analogue of surite, from Inyo County, California. American Mineralogist, 77, 1107–1111.

Liu, J.J., Yang, D., Liu, Z.J., Yang, Y., Yang, D., Feng, C.X, and Xie, H. (2007) The organic geochemistry and biomarkers of the large barium metallogenic belt in the southern Qinling Mountains, China. Journal of Mineralogy and Petrology, 27, 39–48 (in Chinese with English abstract).

Liu, J.J., Wu, S.H., Liu, Z.J., Yang, Y., and Shi, L. (2008a) Sulfur isotopic composition and its geological significance to the large barium metallogenic belt in the northern margins of the Yangtze Block. Bulletin of Mineralogy, Petrology and Geochemistry, 27, 269–275 (in Chinese with English abstract).

Liu, J.J., Liu, Z.J., and Su, W.C. (2008b) Discussion on the origin of the Dabashan witherite deposits, China. Goldschmidt Conference Abstracts, Geochimica et Cosmochimica Acta, 72, A557.

Liu, J.J., Yang, D., Liu, Z.J., Yang, Y., and Mao, G.J. (2008c) Mineralogy of sulvanite from the large barium metallogenic belt in the southern Qinling Mountains, China and its significance. Journal of Mineralogy and Petrology, 28, 44–50 (in Chinese with English abstract).

Liu, J.J., Wu, S.H., Liu, Z.J., Su, W.C., and Wang, J.P. (2010) Discussion on origin of the witherite deposits in large–scale barium metallogenic belt, southern Qinling Mountains, China: Evidence from individual fluid inclusion. Geoscience Frontiers, 17, 222–238 (in Chinese with English abstract).

Lv, Z.C., Liu, C.Q., Liu, J.J., and Zhao, Z.Q. (2003) Carbon, oxygen and boron isotopic studies of Huangbaishuwan witherite deposit at Ziyang and Wenyuhe witherite deposit at Zhushan. Science in China (Ser. D), 46, 1273–1291.

Mandarino, J.A. (1981) The Gladstone–Dale relationship. Part IV. The compatibility concept and its application. The Canadian Mineralogist, 19, 441–450.

Pasteris, J.D., Wopenka, B., Freeman, J.J., Rogers, K., Valsami-Jones, E., Houwen, J.A.M., and Silva, M.J. (2004) Lack of OH in nanocrystalline apatite as a function of degree of atomic order: implications for bone and biomaterials. Biomaterials, 25, 229–238.

Pekov, I.V., Zubkova, N.V., Chukanov, N.V., Pushcharovsky, D.Yu., Kononkova, N.N., and Zadov, A.E. (2008) Podlesnoite $BaCa_2(CO_3)_2F_2$, a new mineral species from the Kirovskii Mine, Khibiny, Kola Peninsula, Russia. The Mineralogical Record, 39, 137–148.

Roberts, A.C., Grice, J.D., Dunning, G.E., and Venance, K.E. (2001) Fencooperite, $Ba_6Fe^{3+}{}_3Si_8O_{23}(CO_3)_2Cl_3 \cdot H_2O$, a new mineral species from Trumbull Peak, Mariposa County, California. The Canadian Mineralogist, 39, 1059–1064.

Rozhdestvenskaya, I.V. and Frank–Kamenetskii, V.A. (1974) Structure of the dioctahedral mica chernykhite. Kristallokhimiya i Struktura Mineralov, 28–33 (in Russian).

Rozhdestvenskaya, I.V. (1979) Refinement of the structure of chernykhite. Kristallokhimiya i Struktura Mineralov, 66–69 (in Russian).

Shi, S.Y., Wen, H.L., Li, B., He, H.L., and Lu, C.F. (2001) Determination of carbon and sulfur in geological samples by high frequency IR-absorption spectrometric method. Rock and Mineral Analysis, 20, 267–271 (in Chinese with English abstract).

Song, J.W., Wang, H., Yang, J.G., and Li, G.R. (2002) Determination of carbon and sulfur in suspended particulates by HF-combustion infrared absorptiometry. Analysis and Testing Technology and Instruments, 8, 170–173 (in Chinese with English abstract).

Tang, J.X., Lin, W.D., Gao, D.R., and Mu, J.L. (1998) The genesis of the Miaozi witherite–barytocalcite–barytodolomite deposit in Wanyuan City, Sichuan Province. Mineral Deposits, 17, 264–276 (in Chinese with English abstract).

Tu, H.K. (1999a) Metallogenic features of barite and witherite deposits in Qinling–Dabashan Region. Geology of Chemical Minerals, 21, 157–162 (in Chinese with English abstract).

——— (1999b) Study on barium deposit zonation in Qinba Mountain areas. Acta Geologica Gansu, 8, 53–57(in Chinese with English abstract).

Vagenas, N.V. and Kontoyannis, C.G. (2003) The case of calcite in dolomitic marble. Vibrational Spectroscopy, 32, 261–264.

Wang, Z.C. and Ye, L.J. (1998) Microbial–organic mineralization and ancient ocean environment of sedimentary barite and witherite. In L.J. Ye, Ed., Micobial–organic Mineralization and the Background, p. 335–352. Ocean Press, Beijing.

Wu, S.H., Liu, J.J., Zhang, N., and Liu, Z.J. (2010a) Metallogenic characteristics for barite and witherite of the large barium metallogenic belt in southern Qinling Mountains, China. Geoscience, 24, 237–244 (in Chinese with English abstract).

Wu, S.H., Liu, J.J., Liu, Z.J., Zhai, D.G., and Yao, M.J. (2010b) Characteristics of fluid inclusions in barite, witherite and barytocalcite from the Shiti barium deposit in southern Shaanxi and their genetic significance. Geology in China, 37, 1469–1479 (in Chinese with English abstract).

Yu, Y.J. and Ning, S. (2002) Using absorption method of infrared-ray from high frequency combustion to determine the contents of carbon and sulphur in barium containing ferroalloy. Angang Technology, 12, 54–55 (in Chinese).

Manuscript received January 7, 2011
Manuscript accepted October 24, 2011
Manuscript handled by Andrew McDonald